



Prognostic and Treatment Guiding Significance of MRI-Based Tumor Burden Features and Nodal Necrosis in Nasopharyngeal Carcinoma

Xi Chen^{1†}, Xun Cao^{2†}, Bingzhong Jing³, Weixiong Xia¹, Liangru Ke⁴, Yanqun Xiang¹, Kuiyuan Liu¹, Mengyun Qiang¹, Chixiong Liang¹, Jianpeng Li⁵, Mingyong Gao⁶, Wangzhong Li¹, Jingjing Miao¹, Guoying Liu¹, Zhuochen Cai¹, Shuhui Lv¹, Xiang Guo¹, Chaofeng Li^{3*} and Xing Lv^{1*}

¹ State Key Laboratory of Oncology in South China, Collaborative Innovation Center for Cancer Medicine, Department of Nasopharyngeal Carcinoma, Sun Yat-sen University Cancer Center, Guangzhou, China, ² State Key Laboratory of Oncology in South China, Collaborative Innovation Center for Cancer Medicine, Intensive Care Unit, Sun Yat-sen University Cancer Center, Guangzhou, China, ³ State Key Laboratory of Oncology in South China, Collaborative Innovation Center for Cancer Medicine, Department of Information Technology, Sun Yat-sen University Cancer Center, Guangzhou, China, ⁴ State Key Laboratory of Oncology in South China, Collaborative Innovation Center for Cancer Medicine, Department of Medical Imaging, Sun Yat-sen University Cancer Center, Guangzhou, China, ⁵ Department of Radiology, Dongguan People's Hospital, Dongguan, China, ⁶ Department of Medical Imaging, The First People's Hospital of Foshan, Foshan, China

OPEN ACCESS

Edited by:

Vincent Vander Poorten,
KU Leuven, Belgium

Reviewed by:

Ivan Tham,
Gleneagles Hospital, Singapore
Davide Farina,
University of Brescia, Italy

*Correspondence:

Xing Lv
lvxing@sysucc.org.cn
Chaofeng Li
lichao@sysucc.org.cn

†These authors have contributed
equally to this work

Specialty section:

This article was submitted to
Head and Neck Cancer,
a section of the journal
Frontiers in Oncology

Received: 23 February 2020

Accepted: 14 August 2020

Published: 11 September 2020

Citation:

Chen X, Cao X, Jing B, Xia W,
Ke L, Xiang Y, Liu K, Qiang M,
Liang C, Li J, Gao M, Li W, Miao J,
Liu G, Cai Z, Lv S, Guo X, Li C and
Lv X (2020) Prognostic and Treatment
Guiding Significance of MRI-Based
Tumor Burden Features and Nodal
Necrosis in Nasopharyngeal
Carcinoma. *Front. Oncol.* 10:537318.
doi: 10.3389/fonc.2020.537318

We aimed to develop a nomogram integrating MRI-based tumor burden features (MTBF), nodal necrosis, and some clinical factors to forecast the distant metastasis-free survival (DMFS) of patients suffering from non-metastatic nasopharyngeal carcinoma (NPC). A total of 1640 patients treated at Sun Yat-sen University Cancer Center (Guangzhou, China) from 2011 to 2016 were enrolled, among which 1148 and 492 patients were randomized to a training cohort and an internal validation cohort, respectively. Additionally, 200 and 257 patients were enrolled in the Foshan and Dongguan validation cohorts, respectively, which served as independent external validation cohorts. The MTBF were developed from the stepwise regression of six multidimensional tumor burden variables, based on which we developed a nomogram also integrating nodal necrosis and clinical features. This model divided the patients into high- and low-risk groups by an optimal cutoff. Compared with those of patients in the low-risk group, the DMFS [hazard ratio (HR): 4.76, 95% confidence interval (CI): 3.39–6.69; $p < 0.0001$], and progression-free survival (PFS; HR: 4.11, 95% CI: 3.13–5.39; $p < 0.0001$) of patients in the high-risk group were relatively poor. Furthermore, in the training cohort, the 3-year DMFS of high-risk patients who received induction chemotherapy (ICT) combined with concurrent chemoradiotherapy (CCRT) was better than that of those who were treated with CCRT alone ($p = 0.0340$), whereas low-risk patients who received ICT + CCRT had a similar DMFS to those who only received CCRT. The outcomes we obtained were all verified in the three validation cohorts. The survival model can be used as a reliable prognostic tool for NPC patients and is helpful to determine patients who will benefit from ICT.

Keywords: MRI-based tumor burden features, nodal necrosis, distant metastasis, treatment, nasopharyngeal carcinoma

INTRODUCTION

Nasopharyngeal carcinoma (NPC) is a typical disease, of which the incidence rate is the highest in Southeast Asia (1). In the early stage, the tumor can be successfully controlled by radiotherapy alone (2), and locoregionally advanced NPC is recommended to be treated with concurrent chemotherapy (3, 4). It has been reported that the 5-year overall survival (OS) has reached 85% (4, 5). However, NPC is prone to recurrence and/or metastasis after certain treatments, which is the main cause of treatment failure and the major cause of mortality of NPC patients (6–8).

In addition, patients in the same clinical stage receiving similar treatments have different survival outcomes. Therefore, it is necessary to build an effective prognostic model to identify patients with a poor prognosis for whom intensive follow-up and adjuvant chemotherapy may bring about more survival benefits. Thus, many efforts have been made to identify risk factors ranging from biomarkers, such as Epstein–Barr virus (EBV) DNA and gene expression, to radiomics (9–13). Multiplanar magnetic resonance imaging (MRI) is one of the methods most extensively used for the precise mapping of the tumor and the accurate evaluation of NPC. In addition to precisely mapping the tumor and defining the T and N stages of NPC, attempts have been made to include information from MRI into the prognostic analysis of cancer (12, 14–17).

Although tumor volume and nodal volume are commonly acknowledged prognostic tumor burden factors (18–20), NPC is an irregular tumor that shows an expansive, infiltrating, or mixed growth pattern. For the expansive growth pattern, tumor volume is highly associated with T stage, while for the infiltrating growth pattern, it is less associated. The nasopharynx is in the subjacent skull base and has a complex anatomy; invasive NPC can infiltrate the cranial nerves through structural channels such as the pterygopalatine fossa, inferior orbital fissure, ethmoid sinus, and foramen lacerum (21–23). NPC patients with small tumor volumes but large extents of invasion might have poor prognosis. In addition to tumor and nodal volume, more information is needed to precisely reflect the tumor burden. Certain prognostic-related structural information reflecting tumor burden, such as the sectional area and vertical dimension, is not being fully utilized. At the same time, induction chemotherapy (ICT) has been shown to be efficient with low toxicity (24–26); however, not all patients benefit from ICT. A more effective prediction model is needed to identify low-risk patients to reduce overtreatment when concurrent chemoradiotherapy (CCRT) would be enough. As previous studies have revealed that nodal necrosis and nodal level are important imaging features and are independent negative prognostic factors for NPC (14, 27–29), we also collected nodal necrosis and nodal level data from MRI. Therefore, in this study, we established an MRI-based tumor burden feature (MTBF) model and developed a nomogram based on MTBF combined with nodal necrosis and some clinical factors to predict distant metastasis in NPC patients. Furthermore, we used this survival model to further explore the relationship between patients with a high risk of poor outcomes and the corresponding therapeutic schedule, which may help in making clinical decisions for individual patients suffering from NPC.

MATERIALS AND METHODS

Study Design and Participants

In this retrospective study, 1640 patients with non-metastatic NPC who were treated at Sun Yat-sen University Cancer Center (Guangzhou, China) from 2011 to 2016 were enrolled. For the inclusion and exclusion criteria of the participants, see **Supplementary Material p 1**. A total of 1148 and 492 patients were randomized to a training cohort and an internal validation cohort, respectively, by computer-generated random numbers [random numbers from 1 to 1640 for each patient, utilizing the function “sample” in R project (version 3.5.2) with a pre-defined seed “250,” and the ratio of training cohort to internal validation cohort size is 7 to 3]. To further validate the generalizability of the model, we enrolled 200 and 257 patients into two external validation cohorts, the Foshan and Dongguan validation cohorts, respectively. The patients in these two external validation cohorts were enrolled following the same criteria. The tumor stage of the enrolled patients was determined in accordance with the 8th edition of the American Joint Committee on Cancer staging manual. This study was carried out with approval of the ethical committees of the Chinese Clinical Trial Registry (ChiECRCT20190127). We have uploaded all crucial research data to the Research Data Deposit public platform (RDDA2020001382).

Procedures

We utilized a Microsoft Excel form to collect sociodemographic information (including age, sex, native place, weight, BMI, and height) and baseline clinical data [EBV DNA before treatment, EA-IgA, VCA-IgA, LYMPH, WBC, RBC, PLT, HGB, total protein (TP), ALB, lactate dehydrogenase (LDH), C-reactive protein (CRP), ABO blood type, RH blood type, T stage, N stage, clinical stage, and therapeutic regimen]. All variables above were categorized based on routine cutoff points in clinical findings and applications. Nodal necrosis (positive vs negative) and nodal level (above the caudal edge of cricoid cartilage vs lower) were also recorded as categorical variables. Tumor burden variables (volume, maximum cross-sectional area, and vertical dimension of the primary tumor and regional lymph nodes, of which the abbreviations are Tv and Lv, Ta and La, and Td and Ld, respectively) were also recorded in the Excel form as continuous variables.

Unenhanced and enhanced head and neck MRI of NPC participants were assessed, and the execution details are presented in **Supplementary Material p 1**. Based on enhanced T1-weighted imaging (T1WI), three specialists in MRI contoured the margin of the primary tumor and regional lymph nodes by utilizing Medical Imaging Interaction Toolkit (MITK) software (version MITK-2016.11.0; **Supplementary Figure 1**). Any disagreements were resolved by a consensus. Detailed information on the calculation of Tv, Lv, Ta, La, Td, and Ld is presented in **Supplementary Materials p 1–2**.

Treatment Methods

All patients underwent radiotherapy. Patients from our center and those in the Foshan validation cohort received

intensity-modulated radiation therapy (IMRT). A total of 2.3% (6 of 257) of the patients in the Dongguan validation cohort received two-dimensional radiotherapy (2D-RT), and 97.7% (251 of 257) of the patients received IMRT. The cumulative radiation doses were 66 Gy or greater in 30–35 fractions, and treatment was delivered once daily, over 5 fractions per week. All patients received platinum-based chemotherapy, including concurrent chemotherapy and ICT. ICT consisted of cisplatin with 5-fluorouracil, taxanes, or both triweekly for two or three cycles. Concurrent chemotherapy consisting of cisplatin was administered weekly or triweekly during radiotherapy.

Follow-Up and Study Endpoints

Follow-up surveys were conducted every 3 months over the first 2 years after radical therapy, once semiannually in the third to fifth years, and once yearly thereafter. The follow-up involved the determination of plasma EBV DNA concentration and indirect or direct nasopharyngoscopy, X-ray/plain and contrast-enhanced CT imaging of the chest, sonography/plain and enhanced CT of the abdomen, and plain and enhanced MRI of the head and neck. In this study, the primary endpoint was distant metastasis-free survival (DMFS), defined as the period from the first day of treatment (radiotherapy or chemotherapy) to the first occurrence of distant metastasis. The second endpoint was progression-free survival (PFS), defined as the period of time from the first diagnosis to locoregional failure, distant failure, or death from any cause, whichever occurred first.

Statistical Analysis

We first carried out univariate analysis on the six tumor burden variables (Tv, Lv, Ta, La, Td, and Ld), in which the p value adopted for excluding variables with least significance was 0.1 ($p > 0.1$). Then, we conducted multivariate Cox regression analysis with a stepwise step to screen out variables that can be used to establish a prognostic model with the coefficients weighted by the Cox model in the training cohort. Stepwise regression introduces the independent variable one by one on the condition that the independent variable is significant after the F test, which is commonly used to eliminate multicollinearity and select the “optimal” regression equation. In the Guangzhou training cohort, the optimal threshold was determined by using X-tile version 3.6.1, a software developed by Yale University, which allows us to divide patients into high- and low-MTBF groups. The thresholds were determined as the values that can generate the maximum chi-square values in the Mantel–Cox test (30).

To further estimate the effect of MTBF (high vs low), nodal necrosis, and nodal level, we also developed three clinical nomograms after univariate analysis. Considering the overlapping information between N stage and nodal level, we included nodal level into the backward multivariate Cox regression with other clinical factors to generate nomogram A. According to Akaike’s information criterion (AIC), sex, age, N stage, clinical stage, and LDH were selected to generate nomogram A to forecast DMFS in the training cohort. Since relevant results show that plasma EBV DNA is a prospective

biomarker in NPC, we developed nomogram B by adding plasma EBV DNA. After that, we developed nomogram C based on nomogram B by integrating MTBF and nodal necrosis.

Then, calibration curves and the concordance index (C-index, proposed by Harrell) were calculated to assess and compare the prediction performance of the nomograms. To further explore the sensitivity and specificity of the prognostic model, we performed time-dependent receiver operating characteristic (ROC) analysis and calculated the area under the curve (AUC). To explore the association of nomogram C with DMFS, we calculated the total risk score for NPC patients based on nomogram C, and the patients were separated into high-risk and low-risk groups according to a cutoff value. Risk stratification was evaluated using Kaplan–Meier analysis, and the survival curves of the high-risk and low-risk groups were compared using the log-rank test. Differences in PFS between the two groups were also assessed.

The univariate and multivariate analyses of DMFS were carried out using the survival package in R (available online). With the stopping rule of AIC, the likelihood ratio test was carried out to apply backward stepwise selection. Then, the nomograms were developed by using the rms package in R (available online), including the coefficients in the multivariable Cox regression model. In this study, R version 3.5.2 and SPSS version 22.0 were adopted for statistical analyses, and a two-sided p value < 0.05 was adopted to indicate differences with statistical significance.

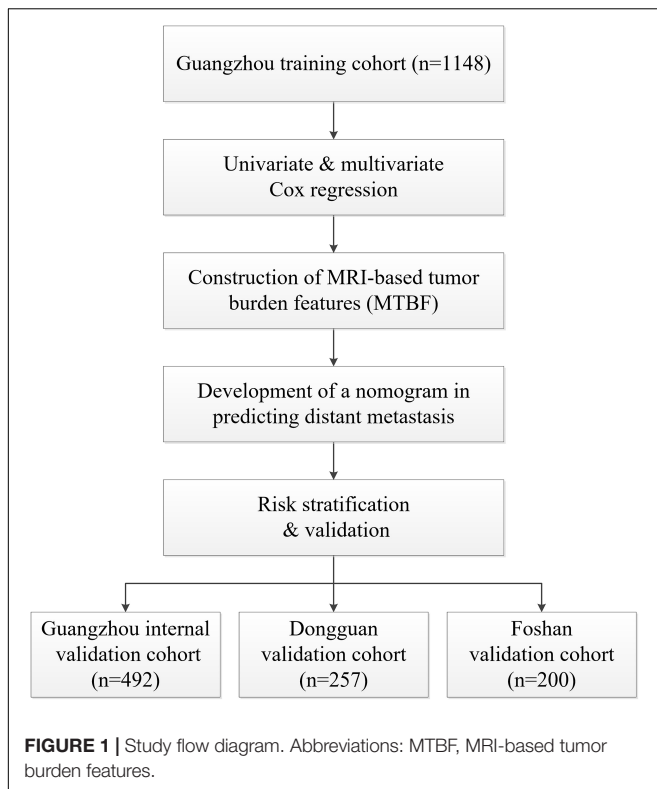
RESULTS

Patient Data and Follow-Up

In total, 2097 patients from three Chinese academic institutions were enrolled. The study flow diagram is shown in **Figure 1**. Among 1640 patients treated at Sun Yat-sen University Cancer Center, 1148 and 492 patients were randomized to a training cohort and an internal validation cohort, respectively. Additionally, we enrolled 200 and 257 patients into two independent external validation cohorts, the Foshan and Dongguan validation cohorts, respectively. The median follow-up of the combined Guangzhou cohort was 55.9 months (IQR 41.4–68.7 months), that of the Dongguan cohort was 49.2 months (IQR 37.4–60.7 months), and that of the Foshan cohort was 42.4 months (IQR 37.3–46.0 months). Up to the last follow-up, 205 (12.5%) patients in the combined Guangzhou cohort, 31 (12.1%) in the Dongguan cohort, and 19 (9.5%) in the Foshan cohort developed distant metastasis. For more information on the patients’ demographic information and baseline clinical characteristics, see **Table 1**.

Construction of the MTBF Model

In the Guangzhou training set, the first multivariate Cox regression analysis with a stepwise step showed that five of the six tumor burden variables, namely, Lv, Ta, La, Td, and Ld, were related to DMFS. In addition, a formula was generated based on the 5 tumor burden features weighted by their respective regression coefficients (**Supplementary Table 1**) to calculate



the tumor burden score for these patients. The formula is as follows:

$$MTBF = -0.0043 \times L_v + 0.1121 \times L_a + 0.0587 \times L_d + 0.0528 \times T_a + 0.0917 \times T_d$$

We generated an optimal threshold (3.2) via X-tile plots to assign the patients in the training cohort into high- and low-MTBF groups (**Supplementary Figure 2**). In this section, 882 (76.8%), and 266 (23.2%) patients in the training cohort, 361 (73.4%), and 131 (26.6%) patients in the Guangzhou internal validation cohort, 204 (79.4%), and 53 (20.6%) patients in the Dongguan external validation cohort, and 162 (81.0%) and 38 (19.0%) patients in the Foshan external validation cohort were divided into the high- and low-MTBF groups, respectively. The result of univariate analysis of MTBF is listed in **Table 2**.

Development and Validation of Nomograms to Predict Survival

All variables were assessed primarily through univariate analysis for DMFS. The predictors included MTBF (high vs low), nodal necrosis (positive vs negative), nodal level (above the caudal edge of cricoid cartilage vs lower), sex, age, N stage, clinical stage, LDH, and plasma EBV DNA (**Supplementary Table 2**). After that, we performed multivariate analysis via a backward step using nodal level, sex, age, N stage, clinical stage, and LDH to predict the DMFS of patients in the training cohort. Sex, age, N stage, clinical stage, and LDH were ultimately selected to generate nomogram A [C-index 0.686, 95% confidence interval

(CI): 0.640–0.732] (**Supplementary Table 3** and **Supplementary Figure 3A**). Because relevant results showed that EBV DNA is a prospective prognostic biomarker of NPC, we used sex, age, N stage, clinical stage, LDH, and EBV DNA to develop nomogram B (C-index 0.702, 95% CI: 0.658–0.746; **Supplementary Table 3** and **Supplementary Figure 3B**). Then, we used the six clinical factors, MTBF, and nodal necrosis to develop nomogram C (C-index 0.741, 95% CI: 0.702–0.780; **Figure 2A**). The calibration curves for 3-year DMFS also performed well in the Guangzhou internal validation set (C-index 0.738, 95% CI: 0.676–0.780), Dongguan external validation set (0.747, 0.678–0.816), and Foshan validation set (0.757, 0.657–0.857; **Figures 2B–E**). Then, we compared the sensitivity and specificity of the three nomograms through ROC analysis and found that nomogram C had a higher AUC value than the other two nomograms (**Figure 3** and **Supplementary Table 4**). The ROC curve of nomogram C vs nomogram B or A reached statistical significance in the Guangzhou data set, but that of nomogram C vs B was not statistically significant in the two external validation sets.

Nomogram C and Risk Stratification

According to the regression coefficients of nomogram C (**Supplementary Table 3**), the patients' risk scores were calculated. The patients were divided into high- and low-risk groups by the optimal cutoff value (4.1) determined by X-tile software. The 3-year DMFS rates in the high- and low-risk groups were 75.1% (95% CI: 69.5–81.0) and 93.4% (95% CI: 91.8–95.1), respectively, [hazard ratio (HR) 4.76, 95% CI: 3.39–6.69; $p < 0.0001$; **Figure 4A**]. Compared with low-risk patients, high-risk patients had shorter PFS (HR 4.11, 95% CI: 3.13–5.39; $p < 0.0001$; **Figure 4E**). In the internal validation set, 381 (77.4%), and 111 (22.6%) patients were divided into the low- and high-risk groups, respectively. The 3-year DMFS (HR 4.22, 95% CI: 2.65–6.70; $p < 0.0001$; **Figure 4B**) and PFS (HR 3.38, 95% CI: 2.32–4.92; $p < 0.0001$; **Figure 4F**) of the high- and low-risk groups were significantly different. In the Dongguan validation cohort, 214 (83.3%), and 43 (16.7%) patients were divided into the low- and high-risk groups, respectively, of which the differences in DMFS (HR 2.16, 95% CI: 0.97–4.84; $p = 0.0550$; **Figure 4C**) and PFS (HR 3.16, 95% CI: 1.77–5.65; $p < 0.0001$; **Figure 4G**) were significant. In the Foshan validation cohort, 173 (86.5%) and 27 (13.5%) of the 200 patients were assigned to the low- and high-risk groups, respectively, and significant differences were also observed. Compared with the low-risk group, the high-risk group had worse DMFS (HR 4.40, 95% CI: 1.73–11.2; $p = 0.0007$; **Figure 4D**) and PFS (HR 5.60, 2.69–11.7; $p < 0.0001$; **Figure 4H**). The numbers of events for the different risk groups in the four cohorts are listed in **Supplementary Table 5**.

Nomogram C and Treatment Direction

In the Guangzhou training cohort, 486 and 439 patients in the low-risk group and 87 and 136 patients in the high-risk group received CCRT and ICT + CCRT, respectively. In the high-risk group, the DMFS of patients treated with ICT + CCRT was longer than that of those treated with CCRT alone (HR 0.60, 95% CI: 0.37–0.97, $p = 0.0340$; **Figure 5A**). However, the treatment effects of ICT + CCRT and CCRT were similar in the low-risk

TABLE 1 | Baseline characteristics.

Variable	Guangzhou training set (n = 1148), n (%)	Guangzhou validation set (n = 492), n (%)	Dongguan validation set (n = 257), n (%)	Foshan validation set (n = 200), n (%)
Age (years)				
<45	541 (47.1)	250 (50.8)	104 (40.5)	82 (41.0)
≥45	607 (52.9)	242 (49.2)	153 (59.5)	118 (59.0)
Sex				
Female	280 (24.4)	112 (22.8)	62 (24.1)	42 (21.0)
Male	868 (75.6)	380 (77.2)	195 (75.9)	158 (79.0)
Tumor stage				
T1	125 (10.9)	62 (12.6)	6 (2.3)	13 (6.5)
T2	210 (18.3)	91 (10.6)	94 (36.6)	33 (16.5)
T3	620 (54.0)	250 (50.8)	120 (46.7)	97 (48.5)
T4	193 (16.8)	89 (18.1)	37 (14.4)	57 (28.5)
Node stage				
N0	178 (15.5)	96 (19.5)	27 (10.5)	42 (21.0)
N1	553 (48.2)	215 (43.7)	68 (26.5)	99 (49.5)
N2	244 (21.3)	104 (21.1)	115 (44.7)	43 (21.5)
N3	173 (15.1)	77 (15.7)	47 (18.3)	16 (8.0)
Clinical stage				
II	204 (17.8)	91 (18.5)	36 (14)	29 (14.5)
III	595 (51.8)	243 (49.4)	140 (54.5)	100 (50.0)
IV	349 (30.4)	158 (32.1)	81 (31.5)	71 (35.5)
HGB (g/L)				
<120	68 (5.9)	17 (3.5)	49 (19.1)	24 (12.0)
≥120	1080 (94.1)	475 (96.5)	208 (80.9)	176 (88.0)
LDH(U/L)				
<245	1061 (92.4)	458 (93.1)	242 (94.2)	186 (93.0)
≥245	87 (7.6)	34 (6.9)	15 (5.8)	14 (7.0)
EBVDNA level (copies/ml)				
<4000	713 (62.1)	317 (64.4)	163 (63.4)	129 (64.5)
≥4000	435 (37.9)	175 (35.6)	94 (36.6)	71 (35.5)
Nodal level				
Above the caudal edge of cricoid cartilage	979 (85.3)	420 (85.4)	212 (82.5)	180 (90.0)
Lower	169 (14.7)	72 (14.6)	45 (17.5)	20 (10.0)
Nodal necrosis				
Negative	1001 (87.2)	430 (87.4)	223 (86.8)	179 (89.5)
Positive	147 (12.8)	62 (12.6)	34 (13.2)	21 (10.5)
Tv (cm ³)				
Median (IQR)	45.1 (30.5–73.6)	46.6 (30.6–75.4)	46.6 (32.7–83.0)	40.9 (28.7–63.5)
Lv (cm ³)				
Median (IQR)	32.2 (5.3–76.2)	31.1 (4.0–71.2)	33.4 (12.4–69.7)	12.8 (0.3–50.3)
Ta (cm ²)				
Median (IQR)	9.8 (7.1–14.6)	10.2 (7.3–14.8)	10.1 (7.3–15.0)	9.6 (6.7–13.6)
La (cm ²)				
Median (IQR)	4.9 (1.2–9.2)	4.7 (1.0–8.5)	4.9 (2.5–8.3)	2.9 (0.6–7.5)
Td (cm)				
Median (IQR)	8.5 (6.6–9.9)	8.8 (7.3–9.9)	8.9 (7.3–10.5)	8.6 (7.4–10.5)
Ld (cm)				
Median (IQR)	12.1 (6.6–17.6)	12.1 (5.7–17.6)	13.0 (7.5–17.2)	9.1 (3.2–13.3)
Treatment				
CCRT	573 (49.9)	235 (47.8)	120 (46.7)	68 (34.0)
IC + CCRT	575 (50.1)	257 (52.2)	137 (53.3)	132 (66.0)

HGB, hemoglobin; LDH, lactate dehydrogenase; EBV DNA, Epstein–Barr virus DNA; Tv, volume of the primary tumor; Lv, volume of the regional lymph nodes; Ta, maximum cross-sectional area of the primary tumor; La, maximum cross-sectional area of the regional lymph nodes; Td, vertical dimension of the primary tumor; and Ld, vertical dimension of the regional lymph nodes.

TABLE 2 | Univariate analysis of MTBF.

	DMFS			PFS		
	HR	95% CI	p value	HR	95% CI	p value
Guangzhou training cohort	4.52	3.21–6.37	<0.0001	4.22	3.22–5.54	<0.0001
Guangzhou internal validation cohort	4.77	2.98–7.65	<0.0001	3.83	2.63–5.58	<0.0001
Dongguan external validation cohort	3.13	1.52–6.46	0.0020	3.37	1.93–5.88	<0.0001
Foshan external validation cohort	5.59	2.27–13.80	0.0002	7.12	3.45–14.70	<0.0001

MTBF, MRI-based tumor burden features; DMFS, distant metastasis-free survival; PFS, progression-free survival; HR, hazard ratio; and CI = confidence interval.

group (Figure 5D). This finding was validated in the internal and combined external validation sets (Figures 5B,C,E,F). Compared with patients not receiving ICT, among all the cohorts, treatment with ICT was also related to an improvement of PFS in patients with high-risk scores but not in those with low-risk scores (Supplementary Figure 4).

DISCUSSION

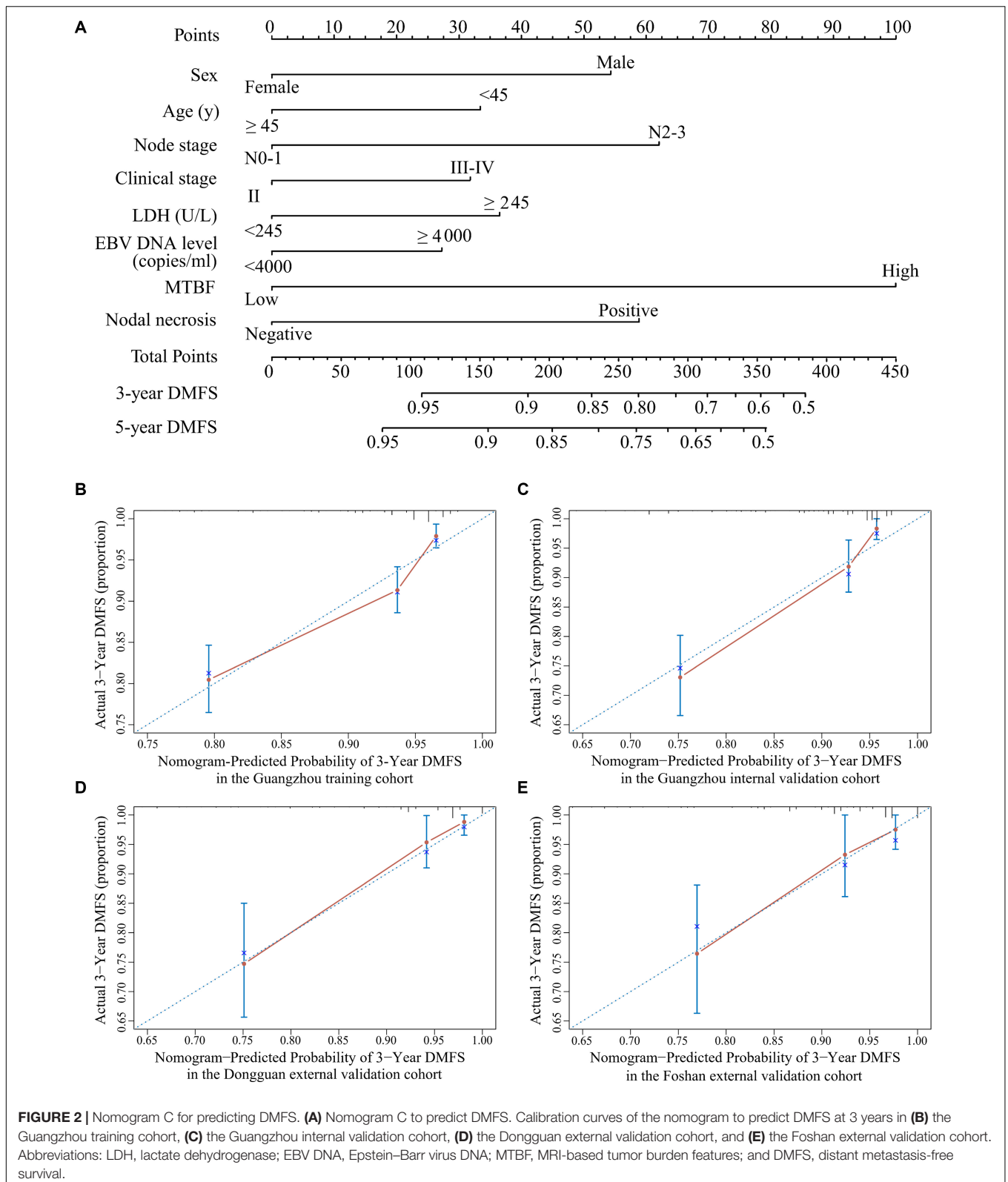
In this retrospective multicenter cohort study, we extracted six multidimensional tumor burden-related variables, including the volume, section area, and vertical dimension of the primary tumor and regional lymph nodes, based on which we developed the MTBF model. Compared to nomogram A (based on routine clinical features) and nomogram B (nomogram A + EBV DNA), nomogram C incorporating MTBF and nodal necrosis to nomogram B had the highest C-index (0.741, 95% CI: 0.702–0.780) and AUC value (0.761, 95% CI: 0.719–0.802). Compared with those of patients in the low-risk group stratified by nomogram C, the DMFS (HR: 4.76, 95% CI: 3.39–6.69; $p < 0.0001$), and PFS (HR: 4.11, 95% CI: 3.13–5.39; $p < 0.0001$) of patients in the high-risk group were relatively poor. Moreover, compared with patients with low risk, treatment with ICT + CCRT tended to have better effects among those with high risk.

Tumor load heterogeneity in the same T and N classification could cause much difficulty for predicting prognosis. Though the volume of the primary tumor is now a commonly acknowledged tumor burden factor for prognosis prediction (18–20), the mining of other information reflecting tumor burden remains insufficient. Our findings, which extracted tumor burden profiles such as the volume, section area, and vertical dimension of the primary tumor and regional lymph nodes based on pretreatment MRI, showed that MTBF is a promising risk factor (HR 4.52, 95% CI: 3.21–6.37; $p < 0.0001$; Supplementary Table 2). Intriguingly, T_v was removed from the construction of the MTBF model during the stepwise regression, whereas the other five tumor burden variables were retained. These results also reflect that the maximum cross-sectional area and vertical dimension could complement the effect of volume on prognosis, which offers more detailed prognostic information. In addition, compared with nomogram A (including sex, age, N stage, clinical stage, and LDH) and nomogram B (including the variables in nomogram A + EBV DNA), the proposed nomogram C (including MTBF, nodal necrosis, and the six variables in nomogram B) achieved

much better performance in terms of the C-index and ROC analysis. Compared with low-risk patients, high-risk patients stratified by nomogram C had poor DMFS (HR: 4.76, 95% CI: 3.39–6.69; $p < 0.0001$) and PFS (HR: 4.11, 95% CI: 3.13–5.39; $p < 0.0001$). With the integration of tumor burden information, nodal necrosis, and other clinical characteristics, MTBF and nodal necrosis were promising supplementary factors to TNM stage and EBV DNA, yielding better performance in predicting survival. As seen in Figure 2A and the coefficients in Supplementary Table 3, MTBF played the most important role in predicting DMFS, and nodal necrosis was also a crucial variable. These results might mainly be associated with two major reasons. First, a high MTBF score and positive nodal necrosis indicate that NPC patients had unfavorable massive primary tumors or regional lymph nodes, which have a greater propensity for occult metastasis (20, 31). Second, massive tumors and positive nodal necrosis have been found to be related to the biological aggressiveness of cancer clones, inadequate blood supply, and other adverse factors, including tumor hypoxia (32, 33), which is strongly associated with radioresistance and thus relapse and metastasis.

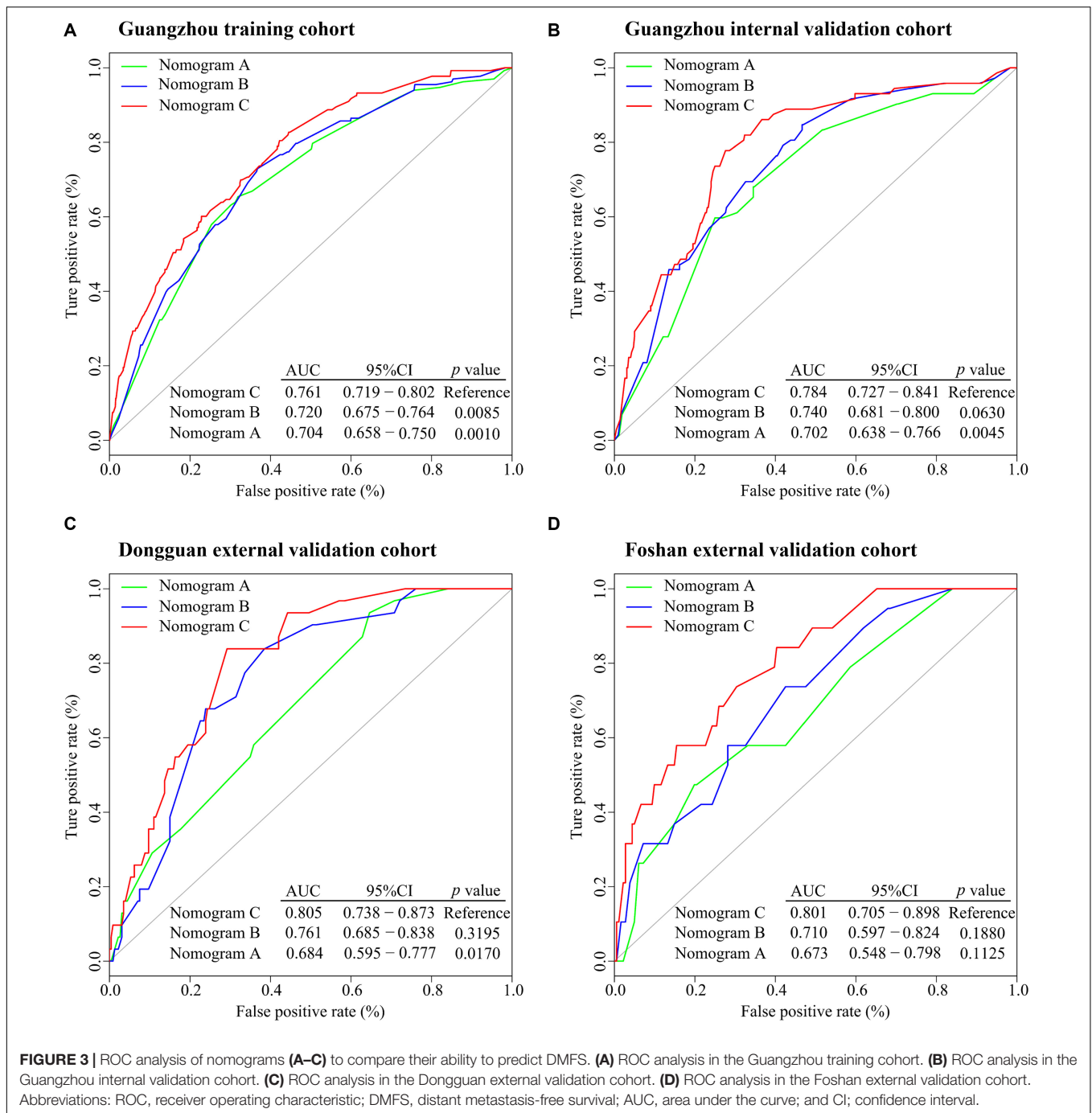
Over 70% of NPC patients are diagnosed with an advanced stage of disease (34, 35). According to the National Comprehensive Cancer Network guidelines, locoregionally advanced NPC patients are at high risk for disease progression, for whom ICT + CCRT is recommended as level 2A evidence and CCRT alone as level 2B evidence. However, not all of these patients benefit from ICT (36). In our investigation, our proposed nomogram model C (including MTBF and nodal necrosis) performed well in predicting survival and succeeded in stratifying high- and low-risk patients who benefited from ICT + CCRT and CCRT, respectively. In the high-risk group, the DMFS of patients treated with ICT + CCRT was longer than that of patients treated with CCRT alone (HR 0.60, 95% CI: 0.37–0.97, $p = 0.0340$; Figure 5A). However, in the low-risk group, the treatment effects of ICT + CCRT and CCRT were similar. This finding might be explained by the fact that ICT not only attenuates tumor load within a brief period to ameliorate tumor hypoxia but also has a systemic cytotoxic effect to eradicate distant micrometastases (37, 38). It is well recognized that the improvement in PFS is mainly due to the reduction in distant metastases. In our study, compared with patients who did not receive ICT, patients with high-risk scores treated with ICT showed an improvement in PFS.

Magnetic resonance imaging is now extensively used for the accurate evaluation of NPC to define the TNM stage and



follow-up, and the majority of NPC patients undergo MRI before treatment. Our prognostic model utilized the information obtained from pretreatment MRI without increasing the physical

or financial burden. One main challenge in our study lies in the fact that three specialists in MRI are required to contour the margin of the primary tumor and regional lymph nodes,



which might take time and effort. Fortunately, with the rise of artificial intelligence, deep learning has been widely applied in radiology and pathology for image processing and lesion recognition (39–42). Automatically recognizing the scope and characteristics of neoplasms will help make our proposed model a more user-friendly prognostic tool. With regard to the result of ROC analysis that the ROC curve of nomogram C vs B was not statistically significant in the two external validation sets, we think the reason lies in the different population distributions and the small sample size. Longer follow-ups and

prospective multicenter clinical studies should be carried out to validate our MTBF model and nomogram. Additionally, radiomics has achieved valuable performance in many prediction tasks, including NPC (16, 43). In addition to structural tumor burden features, nodal level, and necrosis, further investigation incorporating other radiomics data will be our next research interest. In conclusion, the survival model based on MTBF, nodal necrosis, and clinical factors is a promising prognostic tool for NPC and is helpful for identifying patients who might benefit from ICT.

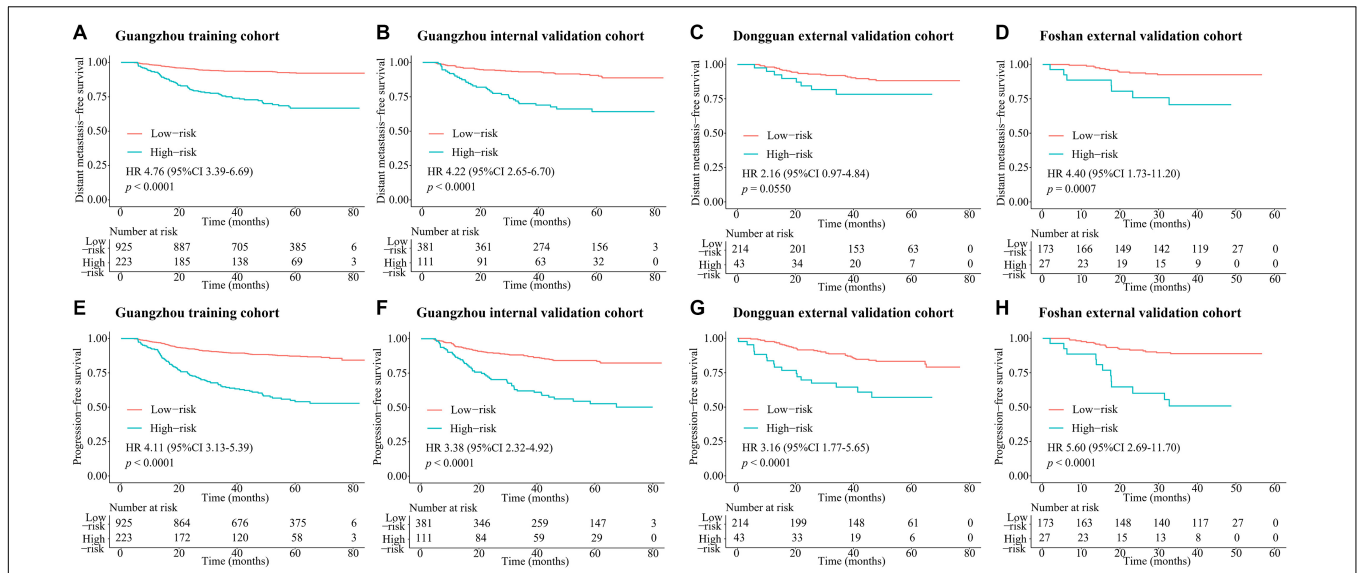


FIGURE 4 | Kaplan–Meier survival curves of DMFS and PFS for risk group stratification with the MTBF. **(A)** DMFS in the Guangzhou training cohort, **(B)** DMFS in the Guangzhou internal validation cohort, **(C)** DMFS in the Dongguan external validation cohort, **(D)** DMFS in the Foshan external validation cohort, **(E)** PFS in the Guangzhou training cohort, **(F)** PFS in the Guangzhou internal validation cohort, **(G)** PFS in the Dongguan external validation cohort, and **(H)** PFS in the Foshan external validation cohort. *P* values were calculated using the unadjusted log-rank test and hazard ratios with a univariate Cox regression analysis. Abbreviations: DMFS, distant metastasis-free survival; MTBF, MRI-based tumor burden features; and HR, hazard ratio.

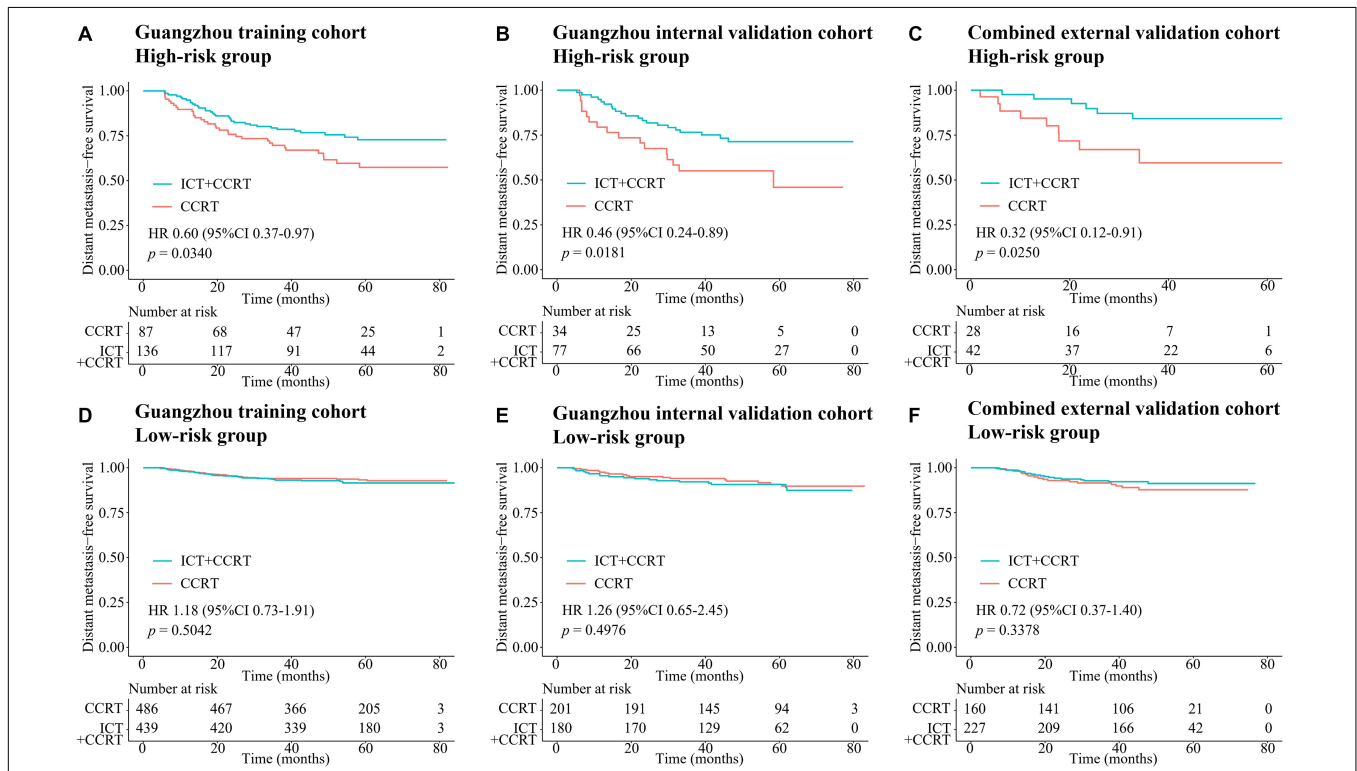


FIGURE 5 | Kaplan–Meier survival curves of DMFS of CCRT alone and ICT + CCRT. **(A)** High-risk group in the Guangzhou training cohort, **(B)** high-risk group in the Guangzhou internal validation cohort, **(C)** high-risk group in the combined external validation cohort, **(D)** low-risk group in the Guangzhou training cohort, **(E)** low-risk group in the Guangzhou internal validation cohort, and **(F)** low-risk group in the combined external validation cohort. Abbreviations: DMFS, distant metastasis-free survival; CCRT, concurrent chemoradiotherapy; and ICT, induction chemotherapy.

DATA AVAILABILITY STATEMENT

The datasets generated for this study are available on request to the corresponding author.

ETHICS STATEMENT

This study was approved by the Ethics Committee of the Chinese Clinical Trial Registry (ChiECRCT20190127). Patients' written informed consent was not required because no direct interaction with patients was performed and no personal identification was applied in this study. In addition, this research was conducted in compliance with the Declaration of Helsinki.

AUTHOR CONTRIBUTIONS

XL, CFL, and XiC designed this study. XiC, MQ, GL, JL, MG, ZC, JM, SL, and WX collected data. LK, XuC, KL, YX, and XG rechecked data. XiC, XuC, BJ, and WL performed analysis and wrote the manuscript. CXL, CFL, and XL helped

to revise the manuscript. All authors approved the final version of the manuscript.

FUNDING

This work was supported by the National Natural Science Foundation of China (Grant Numbers 81872375, 81572665, and 81702873), the International Cooperation Project of Guangdong Science and Technology Program (Grant Numbers 2016A050502011 and 2014A050503033), the Young Teachers Training Project of Sun Yat-sen University (Grant Number 18ykpy35), and the Guangdong Science and Technology Plan Project (Grant Number 2017B020228003). The funders had no influence on the outcomes of this study.

SUPPLEMENTARY MATERIAL

The Supplementary Material for this article can be found online at: <https://www.frontiersin.org/articles/10.3389/fonc.2020.537318/full#supplementary-material>

REFERENCES

- Torre LA, Bray F, Siegel RL, Ferlay J, Lortet-Tieulent J, Jemal A. Global cancer statistics, 2012. *CA Cancer J Clin.* (2015) 65:87–108. doi: 10.3322/caac.21262
- Yi JL, Gao L, Huang XD, Li SY, Luo JW, Cai WM, et al. Nasopharyngeal carcinoma treated by radical radiotherapy alone: ten-year experience of a single institution. *Int J Radiat Oncol Biol Phys.* (2006) 65:161–8. doi: 10.1016/j.ijrobp.2005.12.003
- Chen L, Hu CS, Chen XZ, Hu GQ, Cheng ZB, Sun Y, et al. Concurrent chemoradiotherapy plus adjuvant chemotherapy versus concurrent chemoradiotherapy alone in patients with locoregionally advanced nasopharyngeal carcinoma: a phase 3 multicentre randomised controlled trial. *Lancet Oncol.* (2012) 13:163–71. doi: 10.1016/S1470-2045(11)70320-5
- Blanchard P, Lee A, Marguet S, Leclercq J, Ng WT, Ma J, et al. Chemotherapy and radiotherapy in nasopharyngeal carcinoma: an update of the MAC-NPC meta-analysis. *Lancet Oncol.* (2015) 16:645–55. doi: 10.1016/S1470-2045(15)70126-9
- Yang L, Hong S, Wang Y, Chen H, Liang S, Peng P, et al. Development and external validation of nomograms for predicting survival in nasopharyngeal carcinoma patients after definitive radiotherapy. *Sci Rep.* (2015) 5:15638. doi: 10.1038/srep15638
- Lee AW, Foo W, Mang O, Sze WM, Chappell R, Lau WH, et al. Changing epidemiology of nasopharyngeal carcinoma in Hong Kong over a 20-year period (1980–99): an encouraging reduction in both incidence and mortality. *Int J Cancer.* (2003) 103:680–5. doi: 10.1002/ijc.10894
- Lee AW, Ma BB, Ng WT, Chan AT. Management of nasopharyngeal carcinoma: current practice and future perspective. *J Clin Oncol.* (2015) 33:3356–64. doi: 10.1200/JCO.2015.60.9347
- Xiao WW, Huang SM, Han F, Wu SX, Lu LX, Lin CG, et al. Local control, survival, and late toxicities of locally advanced nasopharyngeal carcinoma treated by simultaneous modulated accelerated radiotherapy combined with cisplatin concurrent chemotherapy: long-term results of a phase 2 study. *Cancer.* (2011) 117:1874–83. doi: 10.1002/cncr.25754
- Ma BB, King A, Lo YM, Yau YY, Zee B, Hui EP, et al. Relationship between pretreatment level of plasma Epstein-Barr virus DNA, tumor burden, and metabolic activity in advanced nasopharyngeal carcinoma. *Int J Radiat Oncol Biol Phys.* (2006) 66:714–20. doi: 10.1016/j.ijrobp.2006.05.064
- Tang LQ, Li CF, Li J, Chen WH, Chen QY, Yuan LX, et al. Establishment and validation of prognostic nomograms for endemic nasopharyngeal carcinoma. *J Natl Cancer Inst.* (2016) 108:djv291. doi: 10.1093/jnci/djv291
- Tang XR, Li YQ, Liang SB, Jiang W, Liu F, Ge WX, et al. Development and validation of a gene expression-based signature to predict distant metastasis in locoregionally advanced nasopharyngeal carcinoma: a retrospective, multicentre, cohort study. *Lancet Oncol.* (2018) 19:382–93. doi: 10.1016/S1470-2045(18)30080-9
- Wan Y, Tian L, Zhang G, Xin H, Li H, Dong A, et al. The value of detailed MR imaging report of primary tumor and lymph nodes on prognostic nomograms for nasopharyngeal carcinoma after intensity-modulated radiotherapy. *Radiother Oncol.* (2019) 131:35–44. doi: 10.1016/j.radonc.2018.11.001
- Peng H, Dong D, Fang MJ, Li L, Tang LL, Chen L, et al. Prognostic value of deep learning PET/CT-based radiomics: potential role for future individual induction chemotherapy in advanced nasopharyngeal carcinoma. *Clin Cancer Res.* (2019) 25:4271–9. doi: 10.1158/1078-0432.CCR-18-3065
- Mao YP, Liang SB, Liu LZ, Chen Y, Sun Y, Tang LL, et al. The N staging system in nasopharyngeal carcinoma with radiation therapy oncology group guidelines for lymph node levels based on magnetic resonance imaging. *Clin Cancer Res.* (2008) 14:7497–503. doi: 10.1158/1078-0432.CCR-08-0271
- Tang L, Li L, Mao Y, Liu L, Liang S, Chen Y, et al. Retropharyngeal lymph node metastasis in nasopharyngeal carcinoma detected by magnetic resonance imaging: prognostic value and staging categories. *Cancer.* (2008) 113:347–54. doi: 10.1002/cncr.23555
- Zhang B, Tian J, Dong D, Gu D, Dong Y, Zhang L, et al. Radiomics features of multiparametric MRI as novel prognostic factors in advanced nasopharyngeal carcinoma. *Clin Cancer Res.* (2017) 23:4259–69. doi: 10.1158/1078-0432.CCR-16-2910
- Shen H, Wang Y, Liu D, Lv R, Huang Y, Peng C, et al. Predicting progression-free survival using MRI-based radiomics for patients with nonmetastatic nasopharyngeal carcinoma. *Front Oncol.* (2020) 10:618. doi: 10.3389/fonc.2020.00618
- Chen MK, Chen TH, Liu JP, Chang CC, Chie WC. Better prediction of prognosis for patients with nasopharyngeal carcinoma using primary tumor volume. *Cancer.* (2004) 100:2160–6. doi: 10.1002/cncr.20210
- Shen C, Lu JJ, Gu Y, Zhu G, Hu C, He S. Prognostic impact of primary tumor volume in patients with nasopharyngeal carcinoma treated by definitive radiation therapy. *Laryngoscope.* (2008) 118:1206–10. doi: 10.1097/MLG.0b013e31816ed587
- Wu Z, Su Y, Zeng RF, Gu MF, Huang SM. Prognostic value of tumor volume for patients with nasopharyngeal carcinoma treated with concurrent

- chemotherapy and intensity-modulated radiotherapy. *J Cancer Res Clin Oncol*. (2014) 140:69–76. doi: 10.1007/s00432-013-1542-x
21. Wong WM, Young SM, Amrith S. Ophthalmic involvement in nasopharyngeal carcinoma. *Orbit*. (2017) 36:84–90. doi: 10.1080/01676830.2017.1279658
 22. Su CY, Lui CC. Perineural invasion of the trigeminal nerve in patients with nasopharyngeal carcinoma. Imaging and clinical correlations. *Cancer*. (1996) 78:2063–9. doi: 10.1002/(sici)1097-0142(199611)78:103.0.co;2-p
 23. Liu L, Liang S, Li L, Mao Y, Tang L, Tian L, et al. Prognostic impact of magnetic resonance imaging-detected cranial nerve involvement in nasopharyngeal carcinoma: a phase 3, multicentre, randomised controlled trial. *Lancet Oncol*. (2009) 115:1995–2003. doi: 10.1002/cncr.24201
 24. Sun Y, Li WF, Chen NY, Zhang N, Hu GQ, Xie FY, et al. Induction chemotherapy plus concurrent chemoradiotherapy versus concurrent chemoradiotherapy alone in locoregionally advanced nasopharyngeal carcinoma: a phase 3, multicentre, randomised controlled trial. *Lancet Oncol*. (2016) 17:1509–20. doi: 10.1016/S1470-2045(16)30410-7
 25. Cao SM, Yang Q, Guo L, Mai HQ, Mo HY, Cao KJ, et al. Neoadjuvant chemotherapy followed by concurrent chemoradiotherapy versus concurrent chemoradiotherapy alone in locoregionally advanced nasopharyngeal carcinoma: a phase III multicentre randomised controlled trial. *Eur J Cancer*. (2017) 75:14–23. doi: 10.1016/j.ejca.2016.12.039
 26. Zhang Y, Chen L, Hu GQ, Zhang N, Zhu XD, Yang KY, et al. Gemcitabine and cisplatin induction chemotherapy in nasopharyngeal carcinoma. *N Engl J Med*. (2019) 381:1124–35. doi: 10.1056/NEJMoa1905287
 27. Feng Y, Cao C, Hu Q, Chen X. Prognostic value and staging classification of lymph nodal necrosis in nasopharyngeal carcinoma after intensity-modulated radiotherapy. *Cancer Res Treat*. (2019) 51:1222–30. doi: 10.4143/crt.2018.595
 28. Lan M, Huang Y, Chen CY, Han F, Wu SX, Tian L, et al. Prognostic value of cervical nodal necrosis in nasopharyngeal carcinoma: analysis of 1800 patients with positive cervical nodal metastasis at MR imaging. *Radiology*. (2015) 276:536–44. doi: 10.1148/radiol.15141251
 29. Ng WT, Lee AW, Kan WK, Chan J, Pang ES, Yau TK, et al. N-staging by magnetic resonance imaging for patients with nasopharyngeal carcinoma: pattern of nodal involvement by radiological levels. *Radiother Oncol*. (2007) 82:70–5. doi: 10.1016/j.radonc.2006.11.010
 30. Camp RL, Dolled-Filhart M, Rimm DL. X-tile: a new bio-informatics tool for biomarker assessment and outcome-based cut-point optimization. *Clin Cancer Res*. (2004) 10:7252–9. doi: 10.1158/1078-0432.CCR-04-0713
 31. Tang LL, Chen YP, Mao YP, Wang ZX, Guo R, Chen L, et al. Validation of the 8th Edition of the UICC/AJCC staging system for nasopharyngeal carcinoma from endemic areas in the intensity-modulated radiotherapy Era. *J Natl Compr Canc Netw*. (2017) 15:913–9. doi: 10.6004/jnccn.2017.0121
 32. Lartigau E, Le Ridant AM, Lambin P, Weeger P, Martin L, Sigal R, et al. Oxygenation of head and neck tumors. *Cancer*. (1993) 71:2319–25. doi: 10.1002/1097-0142(19930401)71:73.0.co;2-c
 33. Janssen HL, Haustermans KM, Balm AJ, Begg AC. Hypoxia in head and neck cancer: how much, how important? *Head Neck*. (2005) 27:622–38. doi: 10.1002/hed.20223
 34. Tang LL, Chen WQ, Xue WQ, He YQ, Zheng RS, Zeng YX, et al. Global trends in incidence and mortality of nasopharyngeal carcinoma. *Cancer Lett*. (2016) 374:22–30. doi: 10.1016/j.canlet.2016.01.040
 35. Mao YP, Xie FY, Liu LZ, Sun Y, Li L, Tang LL, et al. Re-evaluation of 6th edition of AJCC staging system for nasopharyngeal carcinoma and proposed improvement based on magnetic resonance imaging. *Int J Radiat Oncol Biol Phys*. (2009) 73:1326–34. doi: 10.1016/j.ijrobp.2008.07.062
 36. Lan XW, Xiao Y, Zou XB, Zhang XM, OuYang PY, Xie FY. Outcomes of adding induction chemotherapy to concurrent chemoradiotherapy for stage T3N0-1 nasopharyngeal carcinoma: a propensity-matched study. *Onco Targets Ther*. (2017) 10:3853–60. doi: 10.2147/OTT.S133917
 37. Argiris A, Karamouzis MV. Empowering induction therapy for locally advanced head and neck cancer. *Ann Oncol*. (2011) 22:773–81. doi: 10.1093/annonc/mdq426
 38. Langendijk JA, Leemans CR, Buter J, Berkhof J, Slotman BJ. The additional value of chemotherapy to radiotherapy in locally advanced nasopharyngeal carcinoma: a meta-analysis of the published literature. *J Clin Oncol*. (2004) 22:4604–12. doi: 10.1200/JCO.2004.10.074
 39. Esteva A, Kuprel B, Novoa RA, Ko J, Swetter SM, Blau HM, et al. Dermatologist-level classification of skin cancer with deep neural networks. *Nature*. (2017) 542:115–8. doi: 10.1038/nature21056
 40. Mayo RC, Leung J. Artificial intelligence and deep learning – radiology's next frontier? *Clin Imaging*. (2018) 49:87–8. doi: 10.1016/j.clinimag.2017.11.007
 41. Maier A, Syben C, Lasser T, Riess C. A gentle introduction to deep learning in medical image processing. *Z Med Phys*. (2019) 29:86–101. doi: 10.1016/j.zemedi.2018.12.003
 42. Luo H, Xu G, Li C, He L, Luo L, Wang Z, et al. Real-time artificial intelligence for detection of upper gastrointestinal cancer by endoscopy: a multicentre, case-control, diagnostic study. *Lancet Oncol*. (2019) 20:1645–54. doi: 10.1016/S1470-2045(19)30637-0
 43. Qian J, Herman MG, Brinkmann DH, Laack NN, Kemp BJ, Hunt CH, et al. Prediction of MGMT status for glioblastoma patients using radiomics feature extraction from (18)F-DOPA-PET imaging. *Int J Radiat Oncol Biol Phys*. (2020) S0360–3016:31393–6. doi: 10.1016/j.ijrobp.2020.06.073

Conflict of Interest: The authors declare that the research was conducted in the absence of any commercial or financial relationships that could be construed as a potential conflict of interest.

Copyright © 2020 Chen, Cao, Jing, Xia, Ke, Xiang, Liu, Qiang, Liang, Li, Gao, Li, Miao, Liu, Cai, Lv, Guo, Li and Lv. This is an open-access article distributed under the terms of the Creative Commons Attribution License (CC BY). The use, distribution or reproduction in other forums is permitted, provided the original author(s) and the copyright owner(s) are credited and that the original publication in this journal is cited, in accordance with accepted academic practice. No use, distribution or reproduction is permitted which does not comply with these terms.